Supporting Information

Fabrication of 2D/2D BiOBr/g-C_3N_4 with efficiently photocatalytic activity and clarification of its mechanism

Jian Lei [a,1], Xiaomeng Gu [a,1], Peipei Xiao [a,c], Guangzhu Ding [a,*], Yang Yang [a], Xianliang Fu [a], Baihua Long [b,*], Shifu Chen [a], Sugang Meng [a,c*]

[a] Key Laboratory of Green and Precise Synthetic Chemistry and applications, Ministry of Education, College of Chemistry and Materials Science, Huaibei Normal University, Huaibei, Anhui 235000, P. R. China.

[b] College of Material and Chemical Engineering, Pingxiang University, Pingxiang, 337055, P. R. China.

[c] School of Chemistry and Materials Science, University of Science and Technology of China, Hefei, Anhui 230026, China.

* Corresponding author, Tel: +86-561-3802235, E-mail: dinggz@chnu.edu.cn (G. Ding), longbaihua2007@126.com (B. Long), mengsugang@126.com (S. Meng).

[1] These authors contributed equally to this paper.

Materials

Bismuth nitrate pentahydrate ($Bi(NO_3)_3 \cdot 5H_2O$, ≥ 99.0%), potassium bromide (KBr, 99.0%), glacial acetic acid (CH_3COOH, ≥ 99.5%), urea ($CO(NH_2)_2$, 99%), bisphenol A ($C_{15}H_{16}O_2$, ＞ 99%), norfloxacin ($C_{16}H_{18}FN_3O_3$, 98%), sodium sulfate (Na_2SO_4, ≥ 98%), potassium chloride (KCl, 99.8%), potassium ferricyanide ($K_3FeC_6N_6$, 99%), potassium ferrocyanide trihydrate ($K_4FeC_6N_6 \cdot 3H_2O$, ≥ 99.5%), 5,5-Dimethyl-1-pyrroline N-oxide (DMPO, 97%), mannitol ($C_6H_{14}O_6$, 98%), sodium oxalate ($Na_2C_2O_4$, 99%) carbon tetrachloride (CCl_4, ≥ 99.5%) and other used reagents are all analytical reagents and used directly with no further purification.

Preparation of BiOBr/g-C_3N_4 heterojunctions

The g-C_3N_4 was prepared via heating urea at 500 ℃ and 550 ℃ for 2 h, respectively. 2D/2D BiOBr/g-C_3N_4 heterojunctions were fabricated by an *in-situ* self-assembly process (Figure 1). Typically, 0.03 g g-C_3N_4 was dispersed into water by ultrasonic treatment and then 0.195 g KBr was dissolved into g-C_3N_4 suspension (denoted as solution A). 0.795 g $Bi(NO_3)_3 \cdot 5H_2O$ and 9 mL CH_3COOH were added into 91 mL water to get solution B. Under stirring, the solution B was added into the solution A, and aging for 7 h. The precipitate was washed with water and absolute ethanol for several times and dried at 60 °C in a vacuum oven. Thus, 2D/2D BiOBr/g-C_3N_4 contained 0.03 g g-C_3N_4 was obtained and marked as BiOBr/g-C_3N_4-0.03. The BiOBr/g-C_3N_4 with different amount g-C_3N_4 (0.01, 0.1 and 0.3 g) were synthesized by varying the amount of g-C_3N_4 and denoted as BiOBr/g-C_3N_4-0.01, BiOBr/g-C_3N_4-0.1 and BiOBr/g-C_3N_4-0.3, respectively. The pure BiOB can be prepared by the same method without the addition of g-C_3N_4.

Characterization

The crystal phase was determined by a powder X-ray diffraction (XRD, Bruker D8) with Cu Kα radiation. The micro-structure was measured on a field emission scanning electron microscope (FESEM, Regulus 8200) and a transmission electron microscope (TEM, JEM 2100). The element analysis was detected on an energy dispersive X-ray spectroscopy (EDX). The surface chemical states and charge transfer were determined on an in-situ X-ray photoelectron spectrometer (*in-situ* XPS, Thermo Fisher Scientific EscaLab 250Xi). The optical properties were measured on an UV-vis diffuse reflectance spectroscopy (DRS, Shimadzu UV-3600) and a time-resolved photoluminescence (PL) spectrometry (TRPL,

Shimadzu RF530). The work function was detected on Ultraviolet photoelectron spectroscopy (UPS, Thermo ESCALAB 250XI).

Photocatalytic activity test

The photocatalytic activity of the as-prepared sample was evaluated by photocatalytic degradation of BPA and NFA under visible light irradiation. A high uniformity integrated xenon light source (PLS-FX300HU, Beijing Perfectlight) equipped with a cutoff filter of 400 nm was used as the visible light source. Specifically, the 50 mg sample was dispersed into 50 mL BPA (20 ppm) or NFA (5 ppm) aqueous solution and stirred for 30 min in the dark to achieve the equilibrium of adsorption and desorption. Then, 4 mL of mixed suspension was taken out at certain intervals, centrifuged and filtered with polyether sulfone membrane. The supernatants were analyzed by UV-vis spectrophotometer (Shimadzu UV 3600 UV-vis-NIR) and liquid chromatography-mass spectrometry (LC-MS, Agilent 1290UPLC and Agilent QTOF 6550) with waters BEH C18 column (2.1 × 50 mm, 1.7 μm).

Structure and computational details

Density functional theory calculations for the monolayer CN and (001) facet of tetragonal BOB were carried out through the Materials Studio with the CASTEP mode. The Perdew-Burke-Ernzerhof (PBE) form exchange-correlation functional was used within the generalized gradient approximation (GGA). The convergence thresholds for the geometry optimization were set as 5.0×10^{-6} eV $atom^{-1}$ for energy and 0.02 eV $Å^{-1}$ for maximum force. After geometry optimization, the average potential profile was calculated to acquire the work functions of the monolayer CN and (001) facet of tetragonal BOB.

PEC measurements

The photoelectrochemical (PEC) tests were measured on an electrochemical workstation (CHI-660E). A Pt wire and Ag/AgCl (3 M KCl) were used as the counter electrode and reference electrode, respectively. The 3 mg catalyst was ultrasonically dispersed in 400 μL water. Then it was deposited on the fluoride tin oxide (FTO) substrate to serve as the working electrode. A quartz cell filled with 0.2 M Na_2SO_4 aqueous solution (pH = 7) was used as the reaction system for detecting transient photocurrent responses and Mott-Schottky plots. 0.01 M KCl electrolyte containing 0.01 M $K_3[Fe(CN)_6]/K_4[Fe(CN)_6]$ was applied to the test of electrochemical impedance spectroscopy (EIS) Nyquist plots. A 300 W Xe lamp (CEL-

HXF300, Beijing Au-light Co. Ltd., China) equipped with a 400 nm cutoff filter was used as a visible light source.

EPR test

The electron paramagnetic resonance (EPR) spectra were measured on an EPR spectrometer (A300, Bruker, Germany). 5, 5-dimethyl-l-pyrroline N-oxide (DMPO) was used as a spin-trap reagent under visible light to detect reaction intermediates (DMPO-·O_2^- and DMPO-·OH). ·O_2^- and ·OH were tested in methanol and aqueous solution (at room temperature and in air atmosphere), respectively. Instrument settings were as follows. Modulation frequency: 100.00 kHz; modulation amplitude: 1.00 G; time constant: 40.96 ms; conversion time: 40.00 ms; sweep time: 40.96 s. The microwave bridge power and frequency were 5.72 mW and 9.826 GHz, respectively.

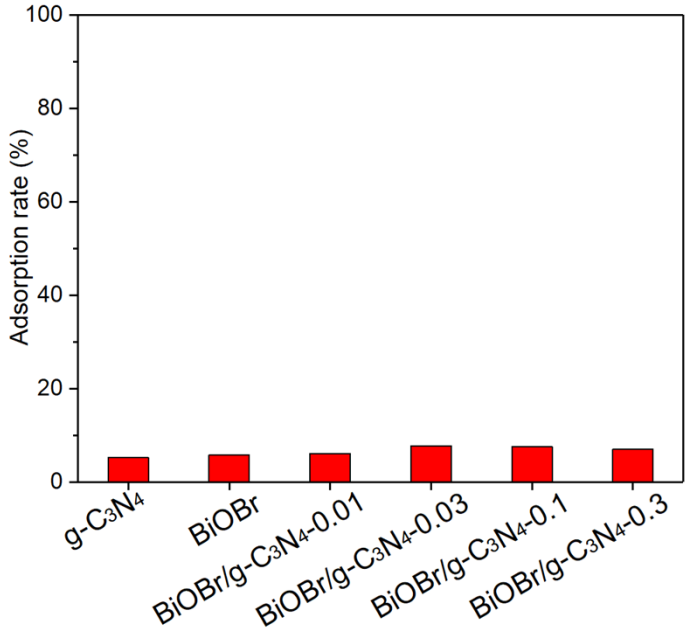

Figure S1. The adsorption rate of BPA on different photocatalysts in the dark.

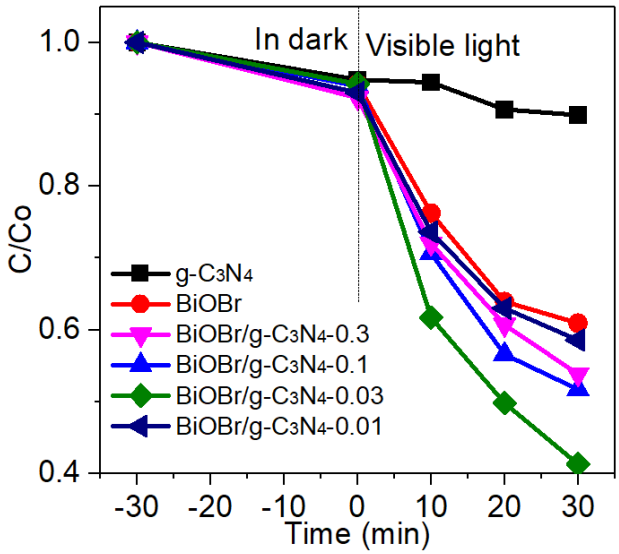

Figure S2. The photocatalytic activities of g-C_3N_4, BiOBr and BiOBr/g-C_3N_4 composites contained with different amount of g-C_3N_4 for photocatalytic degradation of BPA under visible light.

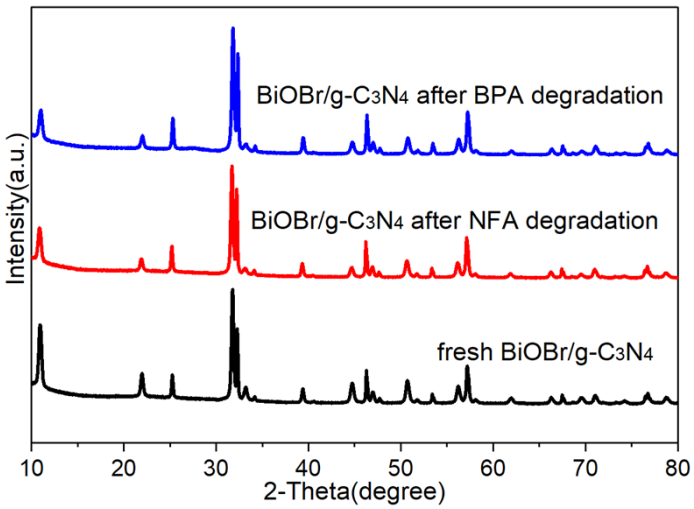

Figure S3. XRD patterns of BiOBr/g-C_3N_4 before and after photocatalytic degradation of BPA and NFA under visible light.

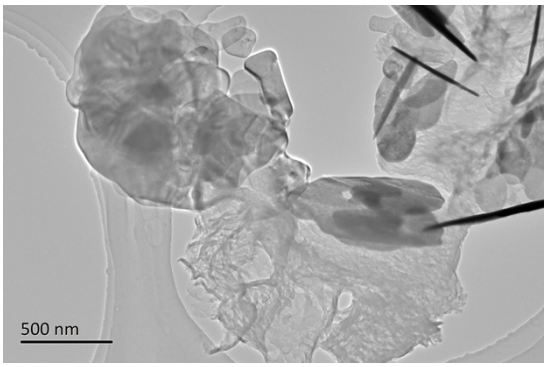

Figure S4. TEM image of BiOBr/g-C_3N_4 after photocatalytic degradation of BPA.

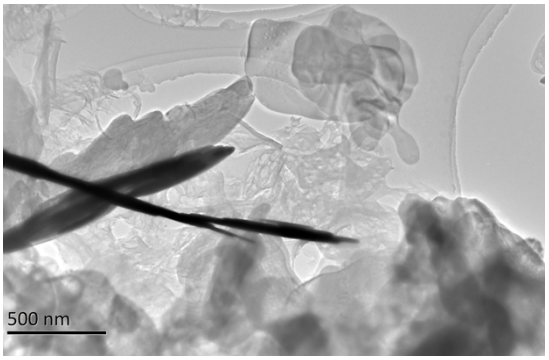

Figure S5. TEM image of BiOBr/g-C_3N_4 after photocatalytic degradation of NFA.

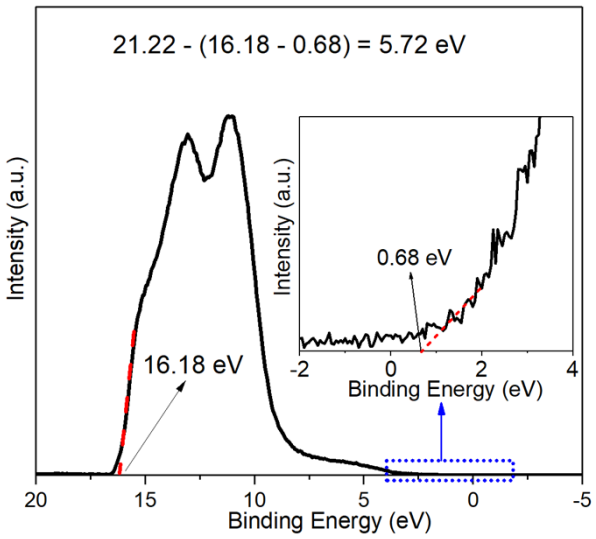

Figure S6. UPS spectrum of g-C_3N_4.

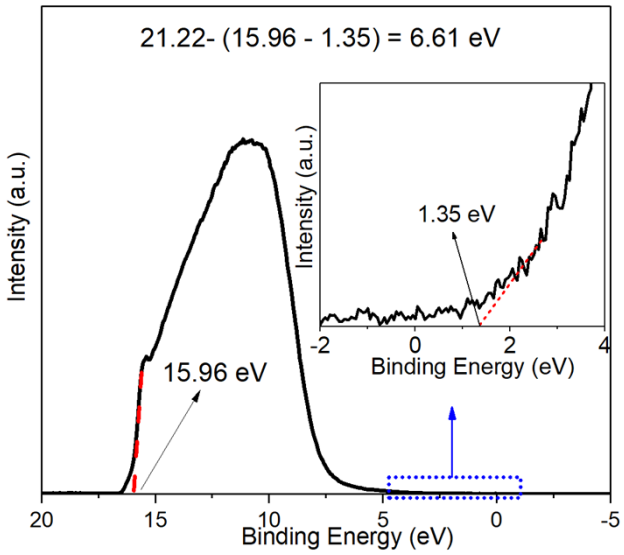

Figure S7. UPS spectrum of BiOBr.

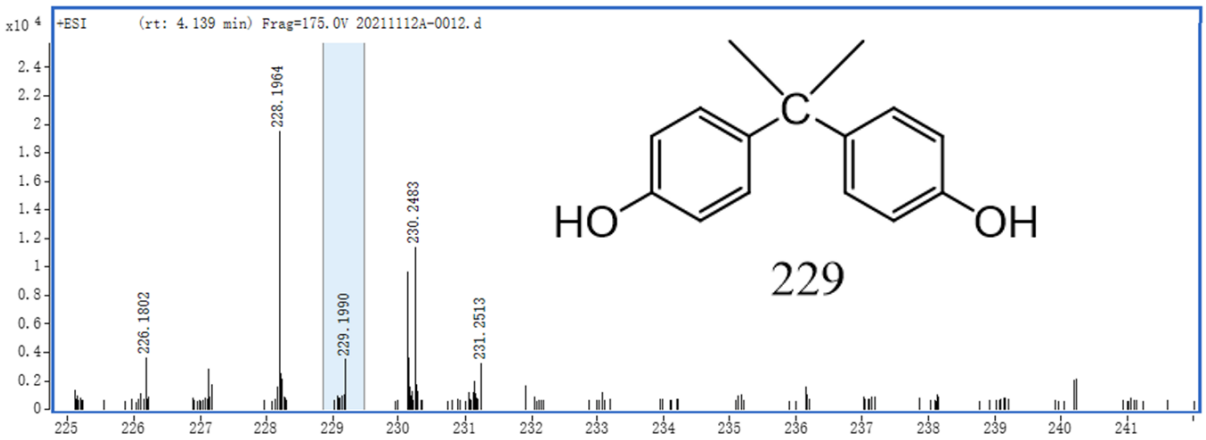

Figure S8. MS spectrum of BPA.

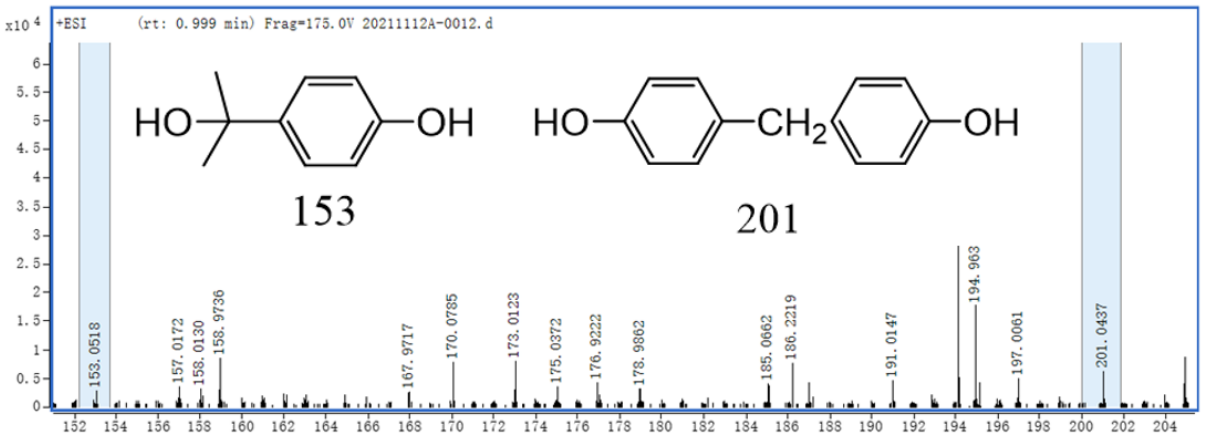

Figure S9. P1 and P4 MS spectrum of BPA degradation on BiOBr/g-C_3N_4 under visible light.

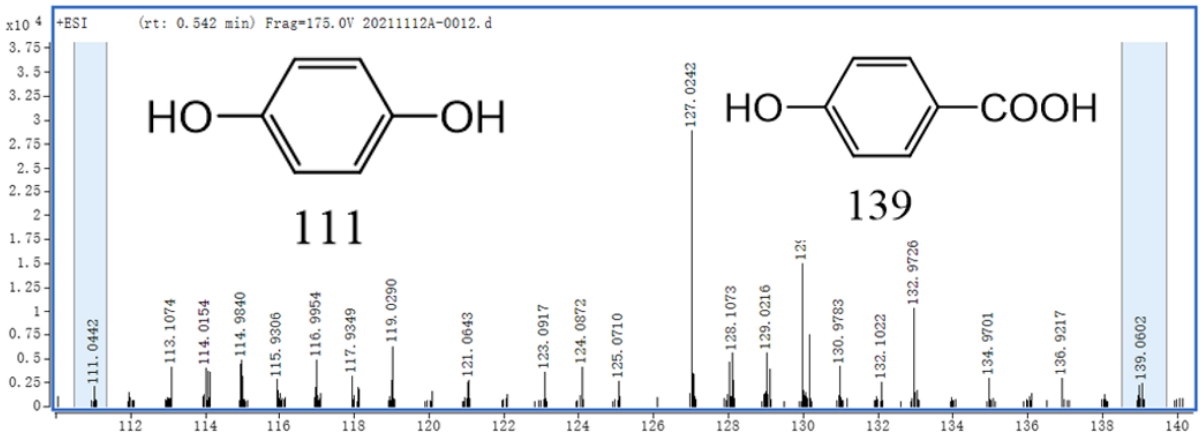

Figure S10. P2 and P3 MS spectrum of BPA degradation on BiOBr/g-C_3N_4 under visible light.

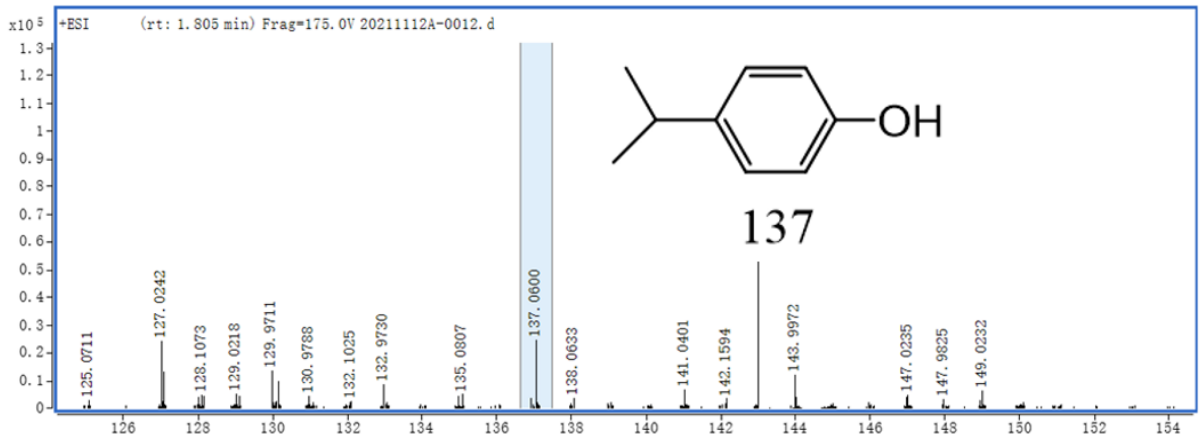

Figure S11. P5 MS spectrum of BPA degradation on BiOBr/g-C_3N_4 under visible light.

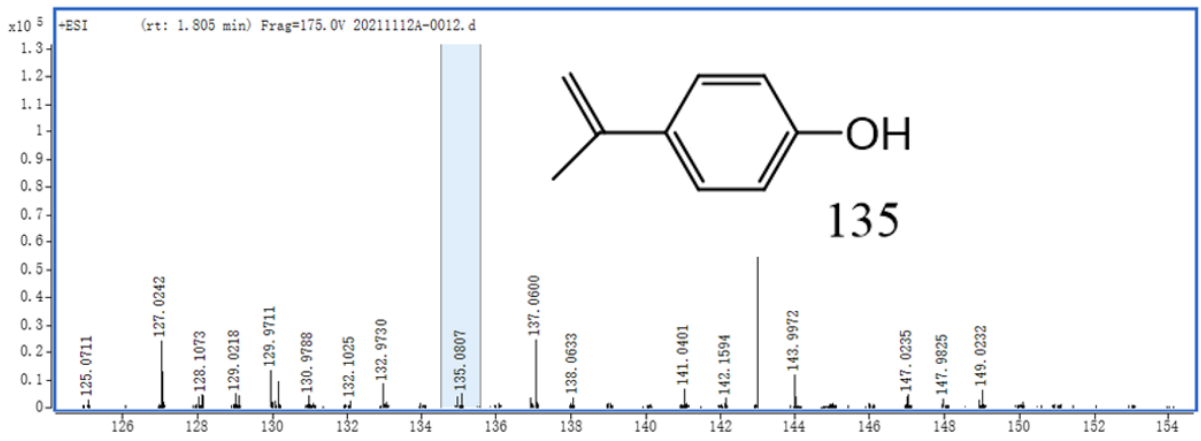

Figure S12. P6 MS spectrum of BPA degradation on BiOBr/g-C_3N_4 under visible light.

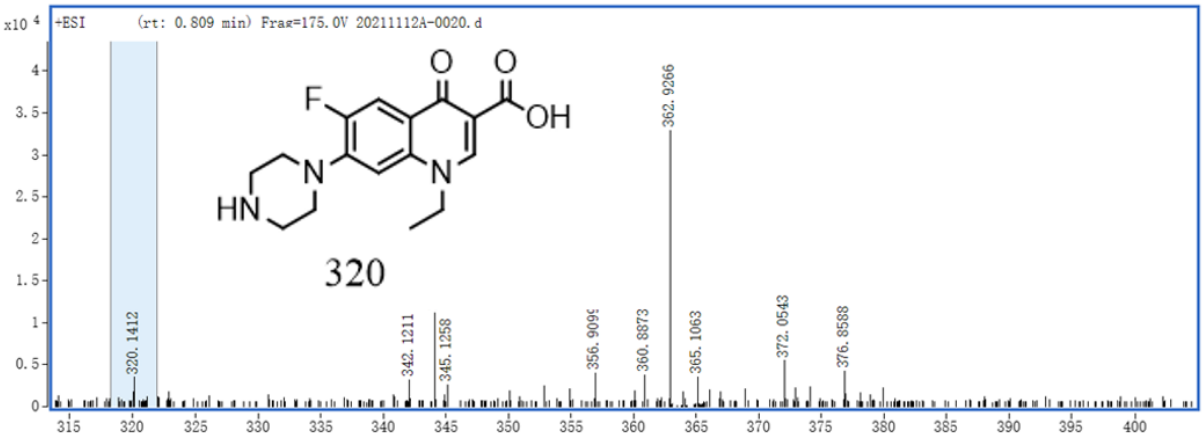

Figure S13. MS spectrum of NFA degradation on BiOBr/g-C_3N_4 under visible light.

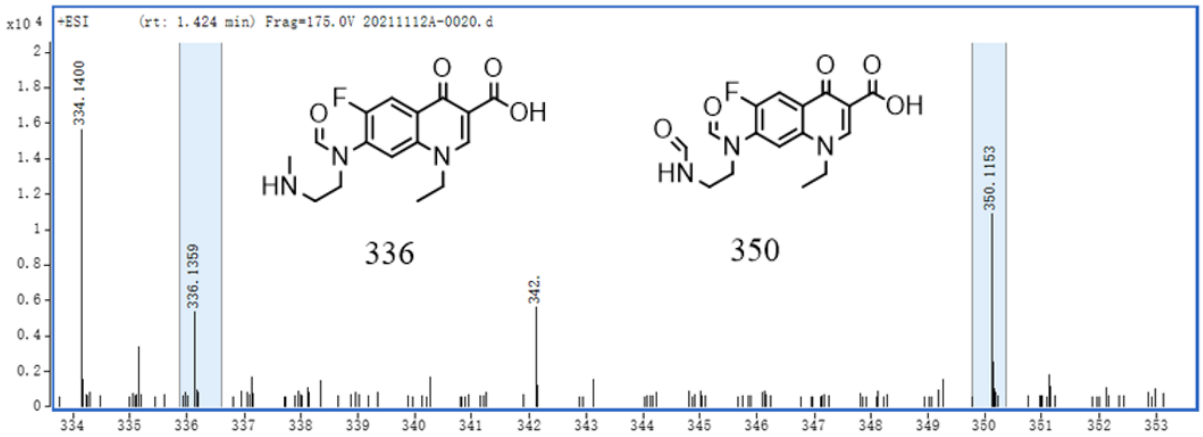

Figure S14. N1 and N2 MS spectrum of NFA degradation on BiOBr/g-C_3N_4 under visible light.

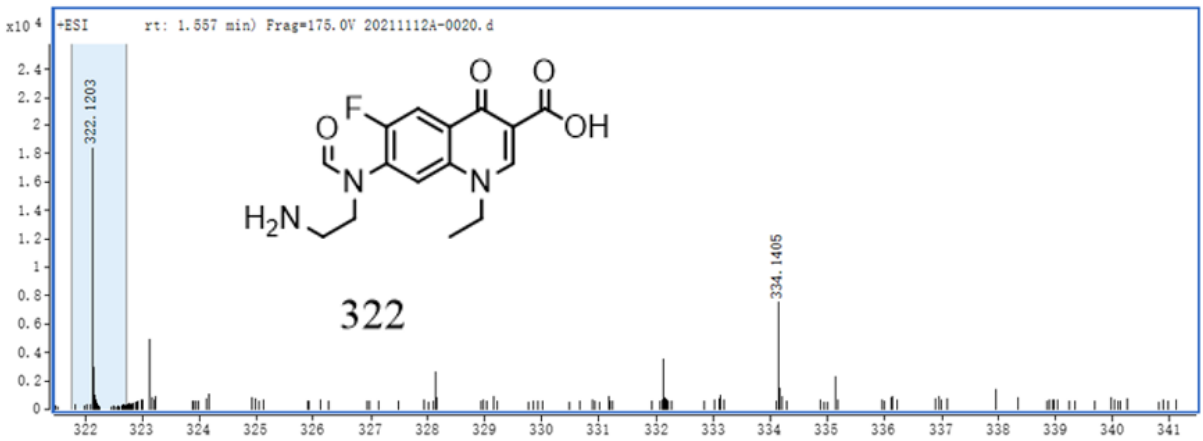

Figure S15. N3 MS spectrum of NFA degradation on BiOBr/g-C_3N_4 under visible light.

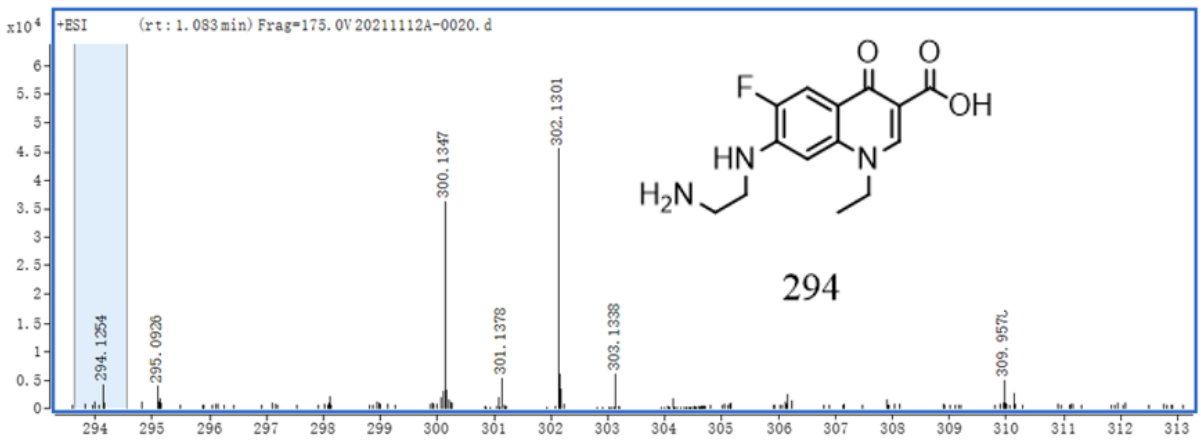

Figure S16. N4 MS spectrum of NFA degradation on BiOBr/g-C_3N_4 under visible light.

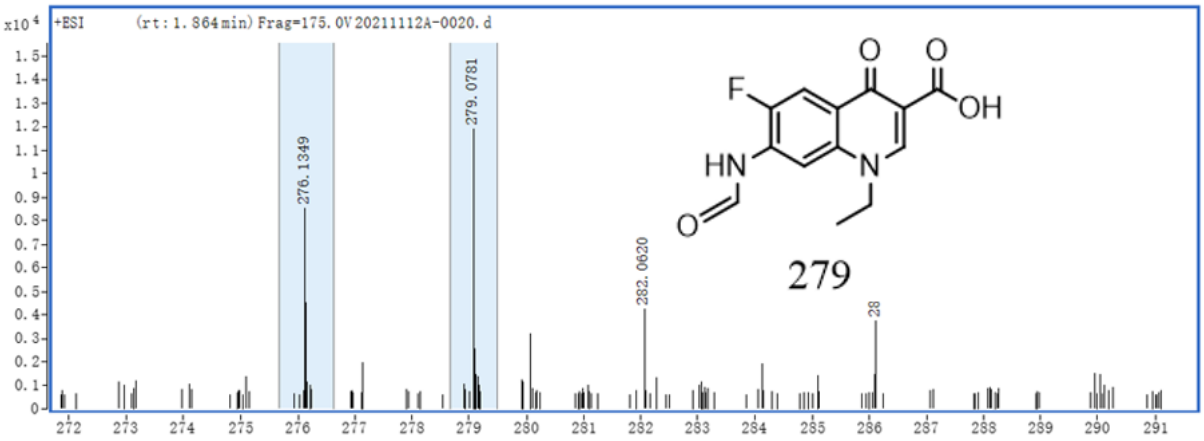

Figure S17. N5 MS spectrum of NFA degradation on BiOBr/g-C_3N_4 under visible light.

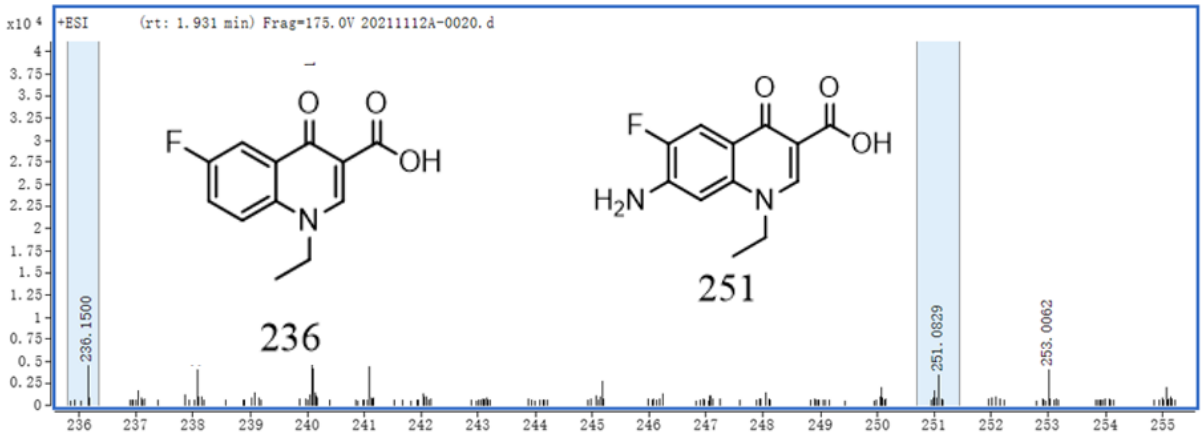

Figure S18. N6 and N7 MS spectrum of NFA degradation on BiOBr/g-C_3N_4 under visible light.

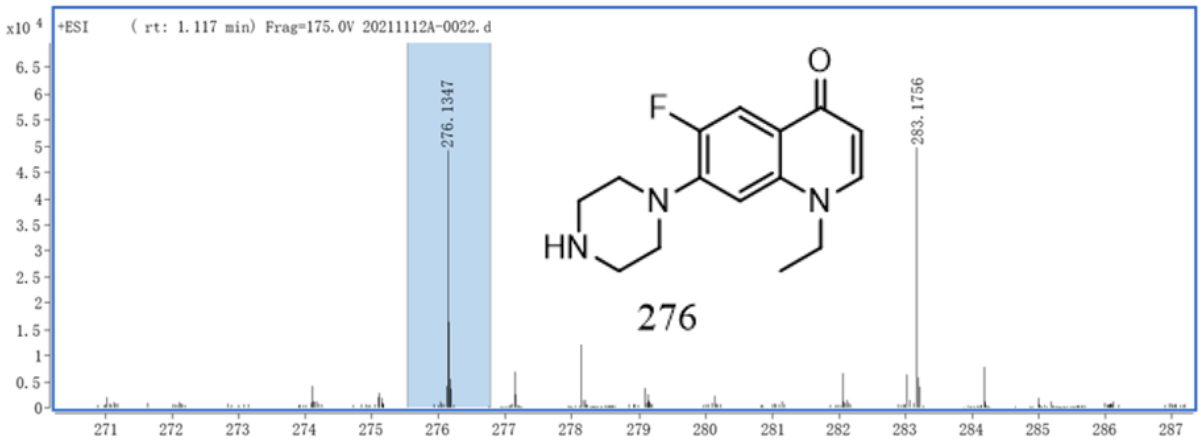

Figure S19. N8 MS spectrum of NFA degradation on BiOBr/g-C_3N_4 under visible light.

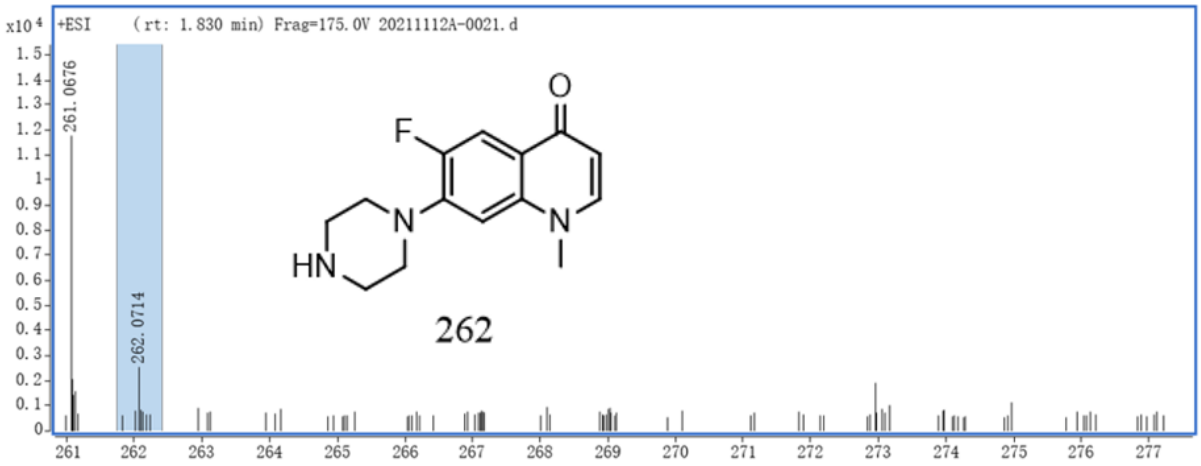

Figure S20. N9 MS spectrum of NFA degradation on BiOBr/g-C_3N_4 under visible light.

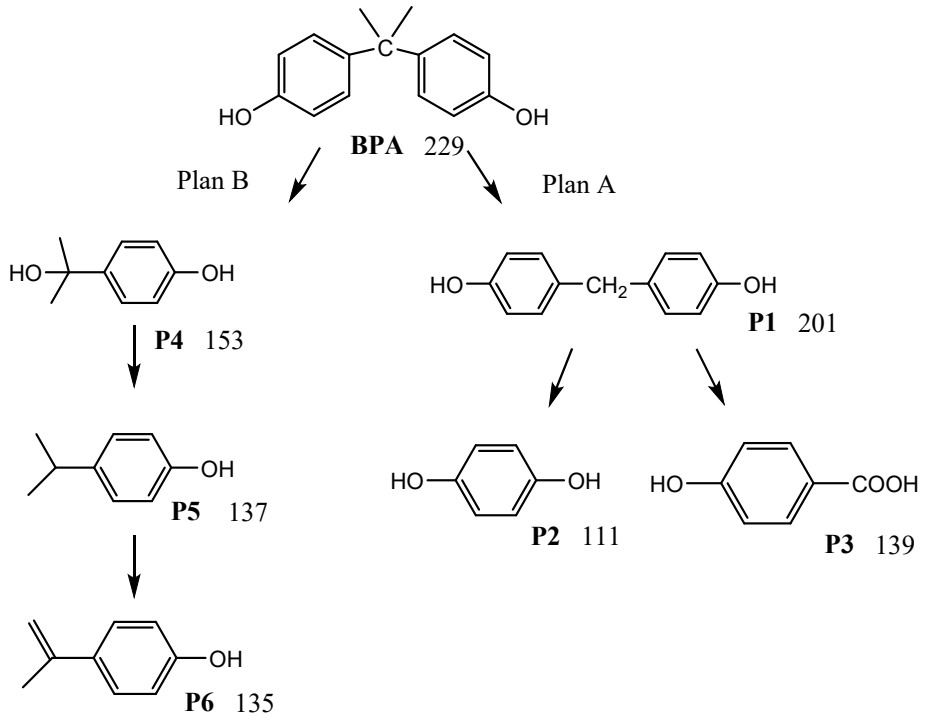

Scheme S1. The possible degradation pathways and intermediates during BPA degradation over BiOBr/g-C_3N_4 under visible light illumination (The numbers 229, 201, 111, 139, 153, 137 and 135 are the value of $[M+H]^+$ *m/z*.).

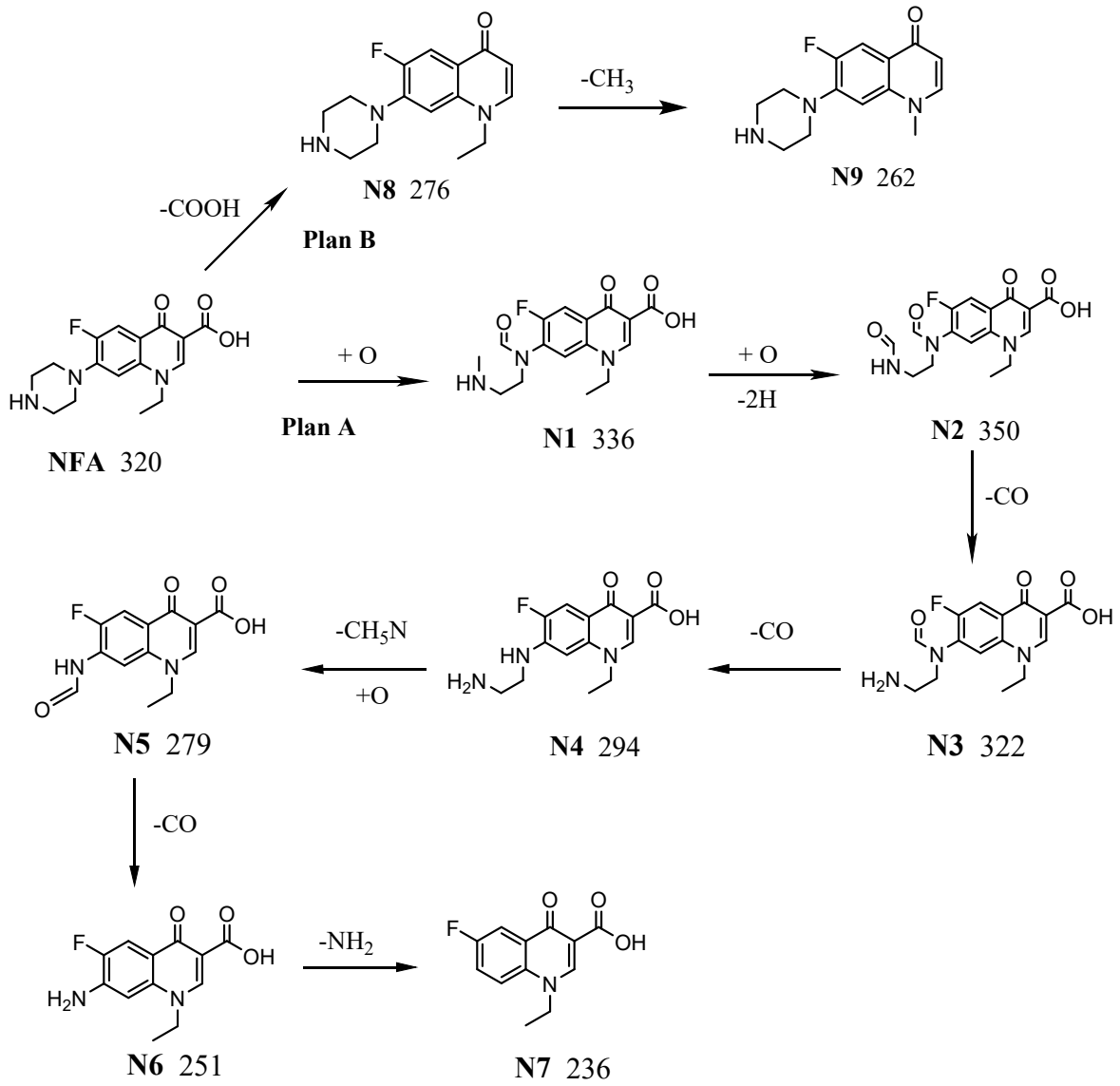

Scheme S2. The possible degradation pathways and intermediates during NFA degradation over BiOBr/g-C_3N_4 under visible light illumination (The numbers 320, 336 and 350, etc., are the value of $[M+H]^+$ *m/z*.).